# Research and Implementation on a Real-Time OSDM MODEM for Underwater Acoustic Communications

Xiaoyu Yang, *Graduate Student Member, IEEE*, Yuehai Zhou, *Member, IEEE*, Rong Wang, and Feng Tong, *Member, IEEE*

***Abstract*—With the increasing demand for marine-sensing information, more and more research has been investigated on underwater wireless sensor networks (UWSNs). Underwater acoustic communication (UWAC) modulators & demodulators (MODEMs) that are used to exchange marine-sensing data have attracted wide attention because they are the most important part of UWSNs. Orthogonal signal-division multiplexing (OSDM) is a compromise between single-carrier communication and multiple-carrier communication. The OSDM communication system is less sensitive to multipath and Doppler shift and has lower peak-to-average power ratio (PAPR). The OSDM UWAC recently has been investigated in theoretical analysis, but as far as we know, there is extremely limited research on real-time OSDM UWAC MODEM design. Aiming at addressing this gap, in this article, a real-time OSDM MODEM is researched and implemented for UWAC, including hardware and software. Specifically, the preamplifier, the bandpass filter, the power amplifier, and the signal processor are introduced. Moreover, detailed procedures for modulation and demodulation are also presented. In addition, to accommodate the different underwater acoustic channels and to get the balance between bit error rate (BER) and data rate, the parameters such as the number of zero vectors and pilot vectors are investigated. Our OSDM MODEM achieves error-free with the data rate of 4.35 kb/s by using the minimum-mean-square-error (MMSE) equalizer and polar decoding under slow time-varying channels, and the communication range reaches larger than 5 km.**

***Index Terms*—Hardware and software design, real-time orthogonal signal-division multiplexing (OSDM) MODEM, underwater acoustic communication (UWAC), underwater wireless sensor networks (UWSNs).**

## I. Introduction

UNDERWATER wireless sensor networks (UWSNs) have attracted wide attention. It plays a pivotal role in many marine applications, such as marine environmental monitoring [1], marine resource exploration [2], data collection [3], marine disaster warning [4], military applications [5], autonomous underwater vehicles (AUVs) [6], and so on. As we know, underwater acoustic communication (UWAC) modulators & demodulators (MODEMs) are the most fundamental and important part of UWSNs. Hence, UWAC MODEMs are researched and implemented in this article.

Compared with wireless channels, underwater acoustic channels are much more complicated. First, radio-frequency electromagnetic waves and optical waves are widely used in terrestrial communication. However, they are rapidly attenuated due to severe propagation loss and scattering in underwater channels. In addition, the attenuation of propagation increases with higher frequencies. As a result, acoustic communication at a frequency below 100 kHz is the only choice for long-range communication [7]. Second, the Doppler effect is responsible for the frequency shift and compresses or expands the signal in the time domain, because of the relative movement between the transmitter and the receiver. Third, due to the gradient of acoustic velocity and nonuniform water, the reflection and refraction result in significant multipath propagation, which may lead to several milliseconds to several hundreds of milliseconds. The delay not only causes serious intersymbol interference (ISI), but also causes frequency selective fading. Fourth, ocean environmental noise is much more

Manuscript received 6 May 2023; revised 24 June 2023; accepted 26 June 2023. Date of publication 7 July 2023; date of current version 15 August 2023. This work was supported in part by the Fundamental Research Funds for the Central Universities under Grant 20720210078 and in part by the National Key Research and Development Program of China under Grant 2018YFE0110000. The associate editor coordinating the review of this article and approving it for publication was Prof. Dongsoo Har. *(Corresponding author: Yuehai Zhou.)*

The authors are with the College of Ocean and Earth Sciences, Xiamen University, Xiamen 361005, China (e-mail: xiaoyuyang@stu.xmu.edu.cn; zhouyuehai@xmu.edu.cn; 22320221151437@stu.xmu.edu.cn; ftong@xmu.edu.cn).

Digital Object Identifier 10.1109/JSEN.2023.3291082

complex, including turbulence, shipping, waves, thermal, and man-made noise. The complex underwater acoustic channels bring great challenges for UWAC.

UWAC MODEMs are an essential component of UWAC technology in many aspects, such as underwater wireless communication networks (UWCNs), UWSNs, the formation and operation of AUVs, and so on. The noncoherent underwater acoustic MODEMs are first designed because of their low complexity. Generally speaking, in noncoherent MODEMs, to address the multipath effect, the duration of one symbol should be longer than that of the multipath delay. Therefore, the bandwidth efficiency and the data rate of noncoherent systems are usually low. Currently, the noncoherence UWAC includes amplitude shift keying (ASK), on-off keying (OOK), frequency shift keying (FSK), frequency hopping, direct sequence spread spectrum (DSSS), M-ary different chirp spread signals (MCSS), and so on.

The ASK acoustic MODEMs with low power and low bit error rate (BER) were designed by using STM32F103 in [8], [9], and [10]. The communication range was limited to 500 m. The OOK acoustic MODEMs were designed for video-capable with a high data rate of more than 1 Mb/s in [11] and [12]. A turbo resampling equalizer and a reprogrammable technology were adopted in [11] and [12], respectively. However, the communication range was limited to only 20 m. Zhao et al. [13] designed a MODEM that achieved the data rate of 500 b/s at the range of 2000 m for UWCNs based on the time division multiple access mechanism. A novel underwater acoustic MODEM prototype based on MCSS was designed in [14]. DSSS acoustic MODEMs have been extensively researched in [15], [16], and [17]. The passive time reversal approach was adopted in [15], which improved the performance in a realistic underwater environment. Zheng et al. [16] used a low-complexity hardware method to compensate Doppler with 1–3 knots in a small-sized AUV. Noncoherent FSK modulation was also applied on UWAC in [18] and [19].

The merit of noncoherent underwater acoustic MODEMs is that they are robust to underwater channels. However, with the increasing demand for high data-rate UWAC, noncoherent systems no longer satisfy the requirement due to their low data rate and low bandwidth efficiency. Coherent systems improve the data rate and the bandwidth efficiency significantly, but coherent UWAC typically requires channel estimation and channel equalization, which result in high complexity. In [20], the turbo equalization algorithms were adopted for a variable-spread-rate DSSS UWAC MODEM based on a digital signal processor (DSP). In [21], a low-power and high-performance underwater acoustic MODEM was designed by integrating Doppler shift compensation, an adaptive equalizer, and a turbo decoder. The MODEM could switch modulation between multiple FSK (MFSK) and multiple phase shift keying (MPSK). As part of the EU FP7 project CADDY, Neasham et al. [22] designed a DSSS underwater acoustic MODEM based on the least mean squares (LMS) algorithm, which could reach the maximum data rate of 1.39 kb/s over 1.6 km. To reduce the computational complexity of equalization, the iterative estimation and equalization by using the turbo principle and soft LMS algorithm were adopted in a single-carrier MODEM in [23]. The satisfactory performance was demonstrated in sea trials, and the best BER was less than $10^{-4}$ over 1000 m. To speed up convergence and improve performance, a low-complexity recursive least-squares (RLS) adaptive filter with dichotomous coordinate descent iterations was adopted in [24]. The experimental results demonstrated that up to 46 dB of self-interference was canceled in the full-duplex binary phase shift keying (BPSK) MODEM. In [25], the algorithm that combined the time reversal with a decision feedback equalizer (DFE) was adopted in SHINKAI6500 using quadrature amplitude modulation (QAM). The MODEM reached the effective data rate of 69.24 kb/s at the vertical range of 3600 m with error-free using the bandwidth of 10 kHz. Considering the deep-sea vertical channel that had a sparse structure, in [26], an improved proportionate normalized minimum-symbol error rate (IPNMSER) algorithm was adopted for adaptive turbo equalization, which outperformed the normalized minimum-symbol error rate (NMSER) algorithm and other well-known proportionate-type algorithms. In [27], the JANUS packet in a BPSK or quadrature phase shift keying (QPSK)-based underwater acoustic MODEM was adopted for high-frequency communication from 100 to 130 kHz, which realized 23 kb/s in a pool.

All the above-mentioned references [8], [9], [10], [11], [12], [13], [14], [15], [16], [17], [18], [19], [20], [21], [22], [23], [24], [25], [26], [27], [28], [29] are single-carrier systems. The multiple-carrier communication MODEMs that are represented by orthogonal frequency division multiplexing (OFDM) also provide an alternative for UWAC. OFDM is the most promising system for UWAC due to its robustness to the multipath effect, high spectral efficiency, and low computational complexity. Hence, many great efforts were taken in [30], [31], [32], [33], and [34]. For example, in [30], an OFDM acoustic communication MODEM was designed, which reached the data rate of 3.1 kb/s. In [31], a multiple-input–multiple-output (MIMO) underwater acoustic MODEM was implemented to achieve the high data rate of 6.4 kb/s by using spatial diversity technology. To overcome the complexity of the underwater environment, Qiao et al. [32] applied many algorithms on OFDM MODEM, including Doppler compensation, channel equalization, and frequency diversity. The MODEM achieved the magnitude of $10^{-3}$ order BER with the data rate of 426 b/s over 36 km in the shallow sea. To achieve the objectives of high throughput rate and high bandwidth efficiency, field reconfigurable and multiuser operation-capable MODEMs were designed, for example, in [33], a full-duplex underwater acoustic MODEM was designed, the MODEM achieved error-free with the data rate of 710 b/s at the distance of 3 km. In [34] and [35], a networked acoustic MODEM system and an HEU OFDM MODEM were also implemented for underwater networks, respectively. To resist the severe fast time-varying multipath interference and environmental noise, an adaptive communication algorithm based on constellation aggregation was implemented in an OFDM MODEM (Seatrix Modem) in [36]. The effectiveness and practicability of the proposed algorithm were demonstrated in the Yellow Sea over 5.5 km.

Because of the complexity of underwater acoustic channels, the single fixed-parameter modulation techniques for

TABLE I
DEVELOPMENT OF UWAC MODEMS IN THE RECENT FIVE YEARS

| Designer | Modulation | Distance (m) | Date rate (kbps) | Bandwidth/Fc (kHz) | BER | Year |
|---|---|---|---|---|---|---|
| Qi Dong [39] | MFSK<br>QPSK | 100<br>100 | 0.208<br>1.23 | 3/12.5 | $10^{-2}$ | 2018 |
| Slamet Indriyanto [18] | FSK | 1.3 | 1.2 | 3/40 | 0 | 2018 |
| Takuya SHIMURA [25] | QAM | 3600 | 69.24 | 10/- | 0 | 2018 |
| Feng Tong [16] | DSSS | 200 | - | 5/16 | - | 2019 |
| Lu Shen [24] | BPSK | 0.04 | - | 1/12 | - | 2019 |
| Yuehai Zhou [7] | OFDM | 1000<br>1200 | 3.55<br>2.663 | 4/16 | $1 \times 10^{-3}$<br>$2 \times 10^{-2}$ | 2019 |
| Yishan Su [19] | DSSS | 2500<br>8000 | 1.07<br>0.125 | -/- | $5 \times 10^{-2}$<br>$3 \times 10^{-2}$ | 2020 |
| Chaohuan Hou [26] | QPSK | 10500 | - | -/- | 0 | 2020 |
| Jinfeng Li [27] | BPSK<br>QPSK | - | 11.5<br>23 | 30/115 | - | 2020 |
| Liang Wang [36] | OFDM | - | 3.765<br>1.882 | -/- | - | 2022 |

underwater acoustic MODEM are not able to accommodate the channel variation. Therefore, many adaptive, reconfigurable, multimode underwater acoustic MODEMs have been investigated. An adaptive MODEM that had six different data rates from 50 to 500 b/s was designed in [37], sea trial demonstrated that the proposed adaptive MODEM could change its modulation schemes and data rate automatically according to channel conditions in real time. In [38], an integrated low-cost underwater sensor node was designed for the reconfigurable FSK MODEM named Proteus II, in which symbol rate, Hamming error correction, and time-of-arrival estimation could be reconfigurable. To accommodate complex underwater acoustic channels, a parameter-configurable OFDM MODEM was designed in [7]. To adapt to highly diverse underwater channels and various missions, the number of receivers, the number of zero subcarriers, and the number of pilot subcarriers were able to be reconfigured, as well as the type of channel estimation algorithms. The effectiveness of the reconfigurable OFDM MODEM was demonstrated by two sea experiments. Different modulation schemes were integrated into a MODEM, for example, a multimode MODEM containing noncoherent and coherent demodulation was implemented in [39].

Recently, software-defined underwater acoustic MODEMs have become a research hotspot due to their flexibility and extensibility. The UNET-2 [40], SEANet [41], and SEANet G2 [42] software-defined MODEMs were introduced. Many underwater acoustic MODEMs are still in laboratory exploitation. So far, there are several commercial underwater acoustic MODEMs, such as Teledyne Benthos, LinkQuest, EvoLogics, Develogic, Kongsberg, SonarDyne, DSPCOMM, AquaSeNT, and so on. A few MODEMs in the last five years are shown in Table I.

Although OFDM has been well implemented in underwater acoustic MODEMs, OFDM systems still suffer from serious peak-to-average power ratio (PAPR) and a high sensitivity to the Doppler effect. On the contrary, single-carrier systems offer lower PAPR and better Doppler tolerance, however, single-carrier systems are very sensitive to multipath and traditionally have high computational complexity due to the time-domain equalizations. As a compromise between single-carrier and OFDM, orthogonal signal-division multiplexing (OSDM) was first proposed in [43] and [44], and further research was carried out for UWAC in [45], [46], [47], [48], [49], [50], and [51].

Recently, OSDM has been applied to underwater acoustic communication. Ebihara and Mizutani [45] compared the OSDM and other existing schemes (single-carrier DFE and OFDM) using simulation and experiment. The excellent communication quality of OSDM with a multichannel receiver in both static and dynamic underwater acoustic channels was verified, which was very competitive with other existing schemes. Ebihara and Leus [46] also proposed Doppler-resilient OSDM (D-OSDM), the results of simulation and test-tank experiments both suggested that the D-OSDM could provide low-power and high-quality communication performance in the underwater channel with severe Doppler and time delay. A lot of efforts focused on underwater acoustic OSDM have been taken in [47], [48], [49], [50], and [51]. In [47], the per-vector channel equalizer and iterative detection were designed to realize intervector interference (IVI) and ISI cancellation, which significantly reduced the computational complexity. To further reduce computational complexity, a low-complexity block and serial OSDM equalization algorithm based on block LDL$^H$ factorization and block iterative matrix inversion was proposed in [48]. To achieve an enhanced frequency diversity gain, a time-domain oversampled OSDM system using multiple virtual channels was designed in [49]. Moreover, an MIMO-OSDM system was proposed to achieve high spectral and power efficiency in [50], and the low-complexity per-vector and block equalization algorithms were proposed to reduce the complexity of channel equalization. To further improve the reliability of the OSDM system under time-varying channels, a joint channel impulse response (CIR) and Doppler estimation algorithm was proposed, instead of an alternating least-squares (ALS) algorithm in [51].

The OSDM communication scheme is a novel high-bandwidth-efficiency technology for UWAC and shows better communication performance. However, this new communication scheme still stays in theoretical analysis [43], [44], [45], [46], [47], [48], [49], [50], [51]. So far, there is no practical underwater acoustic OSDM MODEM. To address this gap and utilize the merits of the OSDM scheme, in this article, a real-time OSDM UWAC MODEM is designed and implemented in an embedded system. The hardware and software parts are designed and implemented in our MODEM. Specifically, the hardware includes a DSP, a power amplifier, an analog-to-digital converter (ADC), a digital-to-analog converter (DAC), preamplifiers, and a bandpass filter. The software includes channel coding, Doppler estimation and compensation, channel estimation, channel equalization, and maximum ratio combining (MRC). To accommodate the different underwater acoustic channels and get the balance between the data rate and performance of our OSDM MODEM, the configuration of the number of zero vectors and pilot vectors is researched in a sea trial. Finally, the performance of the OSDM MODEM is evaluated in terms of BER and equalizer output scatterplots, and the effectiveness of the OSDM MODEM is verified by three sea experiments.

The contribution of our work is the following points.

1) To our best knowledge, this is the first trial that a real-time underwater acoustic OSDM MODEM is designed and implemented in an embedded system.
2) The structure of our underwater acoustic OSDM MODEM is presented, including analog signal processing and digital signal processing.
3) To reduce the computational complexity, new methods that accommodate the embedded system are proposed, and the runtime for different modules is presented.
4) Due to the complex underwater acoustic channels, the research on the balance between data rate and performance with the different numbers of zero vectors and pilot vectors is investigated.
5) The performance of our real-time underwater acoustic OSDM MODEM is demonstrated by three sea trial experiments.

Compared with our previous OFDM MODEM in [7], our proposed OSDM MODEM achieves a longer communication range, better communication performance, and lower PAPR. In addition, since the runtime for demodulating one OSDM symbol is less than that for demodulating one OFDM symbol, the shorter runtime allows the MODEM to use more complex algorithms, for example, using a FARROW filter to resample the large-Doppler OSDM signal on the moving platform.

The remainder of this article is organized as follows: the software design of OSDM MODEM is proposed in Section II. In Section III, the hardware design schemes are introduced in detail. In Section IV, three sea trial experiments are conducted, and the results are analyzed and discussed. In Section V, the conclusion of this article is presented. Finally, future work prospects are in Section VI.

*Notation:* Notation $(\cdot)^*$, $(\cdot)^T$, $(.)^H$, and $(.)^{-1}$ denote conjugate, transpose, Hermitian transpose, and inverse of a matrix, respectively. Notation $\|\cdot\|_2$ denotes L2-norm. Notations $\otimes$ and $\odot$ denote convolution and the Kronecker product, respectively. Notation upper case $\mathbf{X}$ denotes a matrix, and lower case $\mathbf{x}$ denotes a vector. Notations $\mathbf{F}_N$ and $\mathbf{I}_M$ denote the $N \times N$ unitary discrete Fourier transform (DFT) matrix and the $M \times M$ identity matrix, respectively. Notation $\text{diag}(x_0, x_1, \ldots, x_{N-1})$ defines a diagonal matrix with $(x_0, x_1, \ldots, x_{N-1})$ on its diagonal. Similarly, $\text{circ}(\mathbf{x})$ defines a circulant matrix whose first column is $\mathbf{x}$. Notation $\mathbf{0}_N$ defines the $N \times 1$ all-zero vector. Notation $C^{N\times N}$ defines the $N \times N$ matrix in the complex field. Notation $\mathbf{F}_K(:, p:q)$ denotes the submatrix of $\mathbf{F}_K$ from column $p$ to $q$. Notation $\mathbf{i}_N(m)$ denotes the $m$th column of $\mathbf{I}_N$.

## II. Software Design

Our real-time OSDM MODEM includes software and hardware. The flowchart of the UWAC OSDM system is shown in Fig. 1.

Transmission is shown in the top half of Fig. 1. First, the binary sources are encoded by the polar encoding strategy [52], a specific number of binary sources are mapped as a symbol, for example, two binary sources are mapped as QPSK. The OSDM modulation is performed to transform the signal from the frequency domain to the time domain, as shown in Fig. 2. In the time domain, cyclic prefix (CP) adding, upsampling, pulse shaping, and carrier modulation are conducted in sequence. Finally, the OSDM symbols are transmitted to the underwater acoustic channel after the DAC and the power amplifier.

Reception is shown in the bottom half of Fig. 1. The amplitude of received signals from the hydrophone is quite weak, and there are all kinds of ambient noise whose bandwidth may be wide, hence, the preamplifications and the bandpass filter are designed to enlarge the signal and improve the SNR. The analog signal is converted to the digital signal by ADCs. The procedure of processing received digital signals is the opposite of transmission. Carrier demodulation, downsampling, and CP removal are processed in order. The detailed OSDM demodulation of the baseband signals is shown in Fig. 3. The zero vectors are adopted for Doppler estimation, and the pilot vectors are adopted for channel estimation. Symbol demapping and polar decoding are executed after channel estimation and channel equalization.

In this section, the software design of our OSDM MODEM system is introduced, including OSDM modulation, OSDM demodulation, Doppler estimation and compensation, channel estimation, channel equalization, and frame format.

### A. Modulation

In this section, the OSDM system model and the implementation of our OSDM MODEM are introduced step by step. The OSDM system modulation model is shown in Fig. 2. A symbol stream $\mathbf{x}$ with the size of $K_1 = M \times D$ is produced after polar encoding, source coding, and mapping. Different from OFDM systems, in OSDM systems, the $K_1$ symbols are segmented

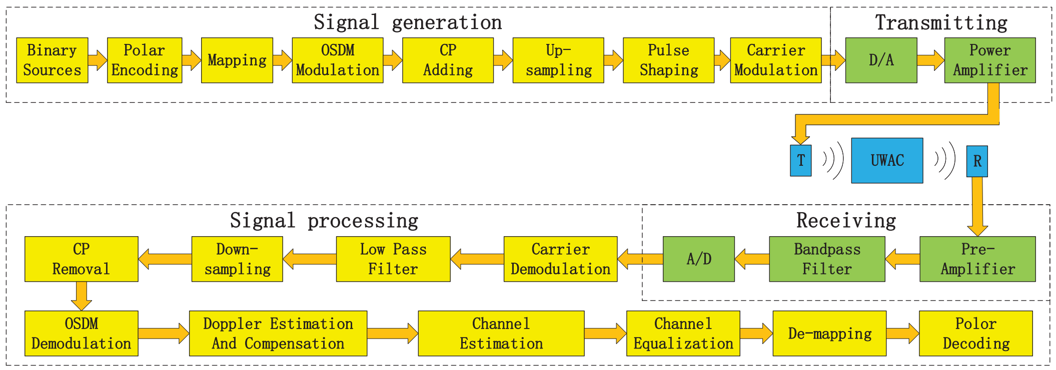


Fig. 1. Flowchart of our UWAC OSDM system.

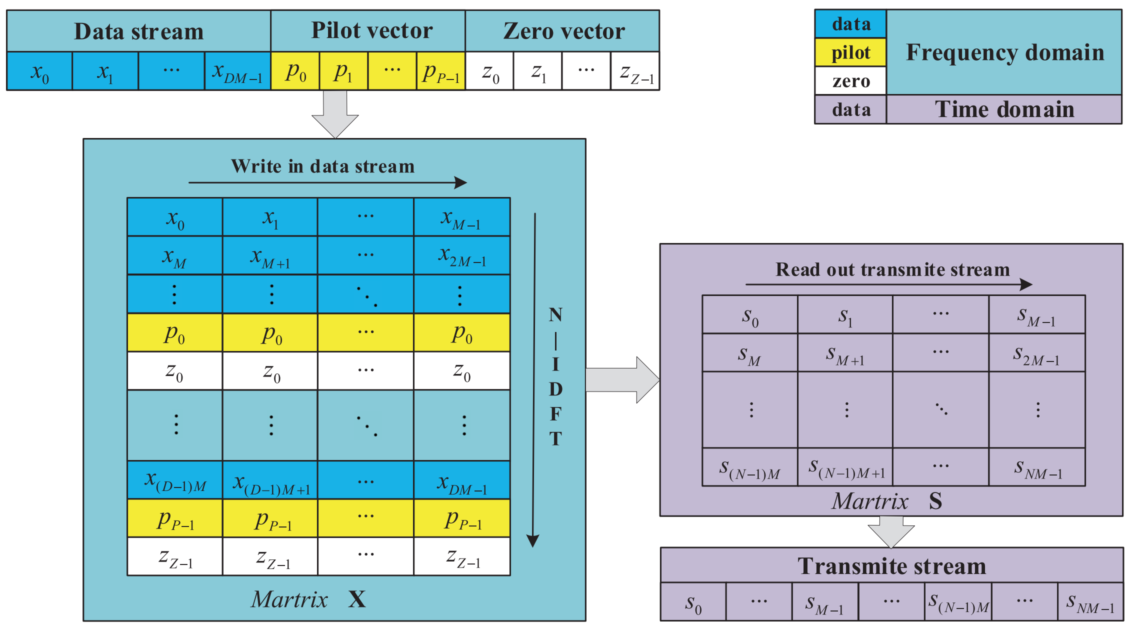


Fig. 2. Structure of OSDM modulation.

into $M$ vectors, and each vector contains $D$ symbols. Then the pilot symbols from the pilot vector $\mathbf{p}$ and the zero symbols from the zero vector $\mathbf{z}$ are inserted sequentially into each data vector, as shown in Fig. 2, hence the length of one vector is $N = D+P+Z$. It is assumed that the index set of data vectors is $S_d = (n_0^d, n_1^d, \ldots, n_{D-1}^d)$, the index set of pilot vectors is $S_p = (n_0^p, n_1^p, \ldots, n_{P-1}^p)$, and the index set of zero vectors is $S_z = (n_0^z, n_1^z, \ldots, n_{Z-1}^z)$. The transmitted symbols can be written in the matrix form $\mathbf{X}$ shown in the following equation:

$$\mathbf{X} = [\mathbf{x}_0, \mathbf{x}_1, \ldots, \mathbf{x}_{M-1}]$$
$$= \begin{bmatrix} x_0 & x_1 & \cdots & x_{M-1} \\ x_M & x_{M+1} & \cdots & x_{2M-1} \\ \vdots & \vdots & \ddots & \vdots \\ p_0 & p_0 & \cdots & p_0 \\ z_0 & z_0 & \cdots & z_0 \\ \vdots & \vdots & \ddots & \vdots \\ x_{(D-1)M} & x_{(D-1)M+1} & \cdots & x_{DM-1} \\ p_{P-1} & p_{P-1} & \cdots & p_{P-1} \\ z_{Z-1} & z_{Z-1} & \cdots & z_{Z-1} \end{bmatrix}. \quad (1)$$

The OSDM modulation process from the frequency domain to the time domain can be expressed as

$$\tilde{\mathbf{s}} = \left(\mathbf{F}_N^H \odot \mathbf{I}_M\right)\tilde{\mathbf{x}} \quad (2)$$

Where $\tilde{\mathbf{x}} = (\mathbf{x}_0^T, \ldots, \mathbf{x}_{M-1}^T)^T$ with the size of $\mathcal{C}^{K\times 1}$, and $K = N \times M$. Equation (2) needs the Kronecker process and needs matrix multiplication with $\mathcal{C}^{K\times K} \times \mathcal{C}^{K\times 1}$. For an embedded system, implementation of (2) costs not only memory, but also CPU resources, which causes long runtime, hence, it is not the optimal choice. In our design, $N$-point inverse DFT (IDFT) is executed, and $M$ times of IDFT are performed. For example, performing $N$-point IDFT for the $k$th vector in $\mathbf{X}$ is characterized as

$$\mathbf{s}_k = \mathbf{F}_N^H \mathbf{x}_k \quad (3)$$

where $\mathbf{s}_k$ is defined as $\mathbf{s}_k=[s_k, s_{M+k}, \ldots, s_{(N-1)M+k}]^T$. Since the DFT matrix $\mathbf{F}_N$ is frequently used in the modulation and demodulation, it is saved in the memory in advance. The computational consumption then needs the multiplication with

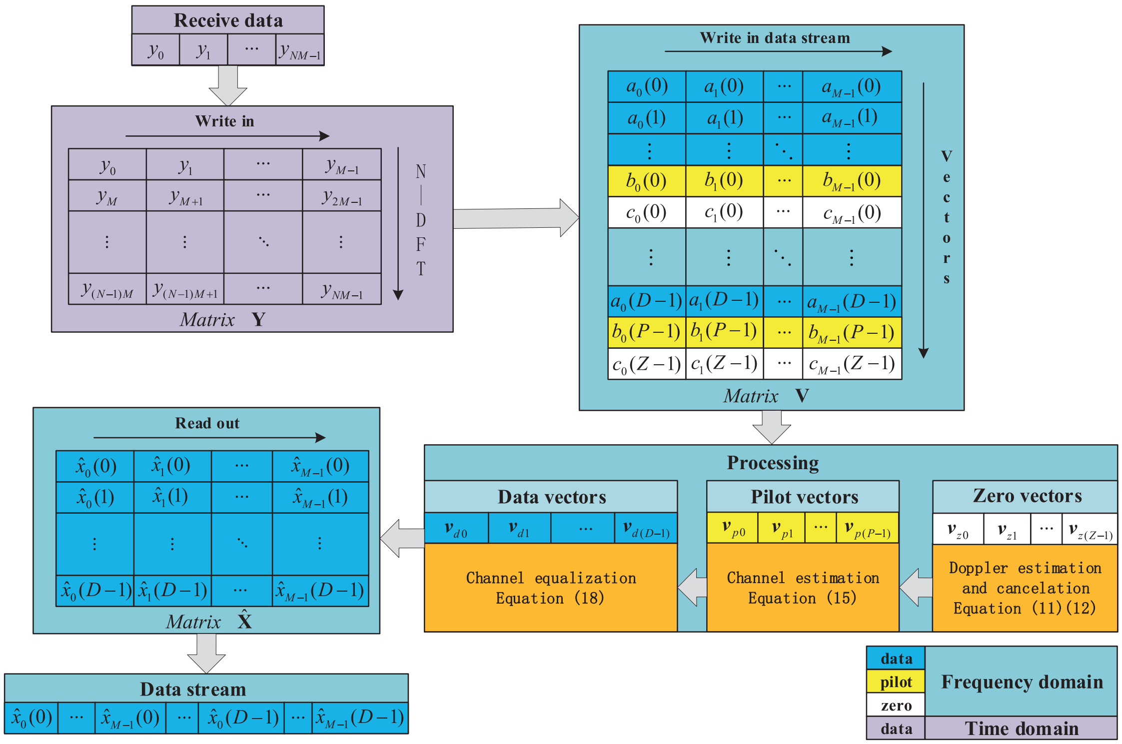


Fig. 3. Structure of OSDM demodulation.

$\mathcal{C}^{M\times N}$, thus the memory and the CPU resources are decreased significantly.

After $M$ times of IDFT, the time-domain transmit matrix is obtained as shown in the following equation:

$$\mathbf{S} = [\mathbf{s}_0, \mathbf{s}_1, \ldots, \mathbf{s}_{M-1}] = \begin{bmatrix} s_0 & s_1 & \cdots & s_{M-1} \\ s_M & s_{M+1} & \cdots & s_{2M-1} \\ \vdots & \vdots & \ddots & \vdots \\ s_{(N-1)M} & s_{(N-1)M+1} & \cdots & s_{NM-1} \end{bmatrix}. \quad (4)$$

Finally, the final OSDM modulation transmission vector $\mathbf{s}$ is generated via reading out the transmission matrix from (4) in a row

$$\mathbf{s} = [s_0, \ldots, s_{M-1}, s_M, \ldots, s_{(N-1)M}, \ldots, s_{NM-1}]^T. \quad (5)$$

Then the signal is transmitted by a transducer after CP adding, upsampling, carrier modulation, the DAC, and the power amplifier, as shown in Fig. 1.

### B. Demodulation

In the receiver, the received signal is distorted because of the complex underwater acoustic channel, for example, the nonnegligible multipath effect and Doppler effect. The digital received signal undergoes carrier demodulation, low-pass filtering, downsampling, and CP removal. Considering the double-selective fading channel, the received time-domain baseband signal can be written as

$$y(i) = e^{(j2\pi i\theta B/K)} s(i) \otimes h(i) + w(i) \quad (6)$$

where $y(i)$, $h(i)$, and $w(i)$ are the discrete signal, channel, and ambient noise, respectively. Notation $i$ denotes the symbol index, $\theta$ denotes the Doppler in Hz, and $B$ denotes the bandwidth.

It is assumed that the multipath and the Doppler keep constant within one OSDM symbol, and it is also assumed that the Doppler shift is uniform among all paths. Equation (6) can be written in vector-matrix form, for example,

$$\mathbf{y} = \mathbf{\Theta}\mathbf{H}\mathbf{s} + \mathbf{w} \quad (7)$$

where $\mathbf{\Theta}$ is defined as $\mathbf{\Theta} = \text{diag}(e^{j2\pi 0\theta B/K}, \ldots, e^{j2\pi(K-1)\theta B/K})$, which is $K \times K$ diagonal phase distortion. Notation $\mathbf{H}$ is defined as $\mathbf{H} = \text{circ}(\mathbf{h}^T, \mathbf{0}^T_{K-L-1})^T$, which is a $K \times K$ circulant CIR matrix. Notation $\mathbf{h}$ is defined as $\mathbf{h} = (h_0, \ldots, h_{L-1})^T$, where $L$ is the channel length. Notation $\mathbf{w}$ is defined as $\mathbf{w} = (w_0, \ldots, w_{K-1})^T$.

Traditionally, to obtain the frequency-domain signal from (7), the DFT is performed

$$\mathbf{q} = (\mathbf{F}_N \odot \mathbf{I}_M)\mathbf{y}. \quad (8)$$

Analogously, implementation of (8) costs large memory and CPU resources.

To simplify the process that transforms the signal from the time domain to the frequency domain, the OSDM demodulation in Fig. 3 is implemented by a three-step process. First, the received signal $\mathbf{y}$ is segmented into $M$ vectors with the size of $N$. At $k$th received vector, it can be denoted as

$$\mathbf{r}_k = (y_k, y_{M+k}, \ldots, y_{(N-1)M+k})^T. \quad (9)$$

Then the $N$-point DFT is performed, such as $\mathbf{q}_k = \mathbf{F}_N \mathbf{r}_k$. Since $\mathbf{F}_N$ is constant, it is written into a ".c" file in advance. The data subcarriers, pilot subcarriers, and zero subcarriers are easy to obtain from $\mathbf{q}_k$. After $M$ times of DFT, all the data subcarriers, pilot subcarriers, and zero subcarriers are fetched via $\mathbf{a}_k = \mathbf{P}_d\mathbf{q}_k$, $\mathbf{b}_k = \mathbf{P}_p\mathbf{q}_k$, and $\mathbf{c}_k = \mathbf{P}_z\mathbf{q}_k$, where $\mathbf{P}_d$, $\mathbf{P}_p$, and $\mathbf{P}_z$ are the selection matrices. In fact, in our design, we do not need the selection matrices, since the positions of data subcarriers, pilot subcarriers, and zero subcarriers are known, and the corresponding subcarriers are easily fetched from $\mathbf{q}_k$ to form vectors. As a result, the memory and the CPU resources are saved. The $m$th data vector, $m$th pilot vector, and $m$th zero vector can be formed as

$$\mathbf{v}_{d_m} = (\mathbf{a}_0(m), \mathbf{a}_1(m), \ldots, \mathbf{a}_{M-1}(m))^T \quad m = 0, 1, \ldots, D-1 \tag{10a}$$

$$\mathbf{v}_{p_m} = (\mathbf{b}_0(m), \mathbf{b}_1(m), \ldots, \mathbf{b}_{M-1}(m))^T \quad m = 0, 1, \ldots, P-1 \tag{10b}$$

$$\mathbf{v}_{z_m} = (\mathbf{c}_0(m), \mathbf{c}_1(m), \ldots, \mathbf{c}_{M-1}(m))^T \quad m = 0, 1, \ldots, Z-1. \tag{10c}$$

After obtaining all the data vectors, pilot vectors, and zero vectors, Doppler estimation and compensation, channel estimation, and channel equalization are performed sequentially.

*1) Doppler Estimation and Compensation:* If the Doppler is not compensated, the vectors will be contaminated which is caused by IVI, thus degrading the performance of channel estimation and channel equalization. In our OSDM MODEM design, it is assumed that the Doppler remains the same within one OSDM symbol, and varies among different symbols. Hence, Doppler estimation and compensation can be performed symbol by symbol. To measure the Doppler, the goal is to minimize the energy of the zero vectors by compensating different tentative Doppler, and therefore, a cost function can be formulated as

$$f(\theta) = \underset{\theta}{\operatorname{argmin}} \left\{ \sum_{k=0}^{Z-1} \|\mathbf{P}_z\mathbf{F}_N\boldsymbol{\Theta}(\theta, k)\mathbf{r}_k\|_2^2 \right\} \tag{11}$$

where $\boldsymbol{\Theta}(\theta, k)$ is defined as $\boldsymbol{\Theta}(\theta, k) = \mathrm{diag}(e^{-j2\pi k\theta B/K}, e^{-j2\pi(k+M)\theta B/K}, \ldots, e^{-j2\pi((N-1)M+k)\theta B/K})$. The tentative Doppler is usually symmetric, for example, from $-\epsilon$ to $\epsilon$, and the Doppler resolution is $\rho$, then (11) is performed $2\epsilon/\rho + 1$ times. To reduce the complexity, the bisectional method is utilized.

In our design, the initial tentative Doppler is from $-20$ to 20 Hz, the initial Doppler resolution $\rho_0 = 4$ Hz, and iter $=$ 10. Hence, the final resolution of Doppler is $\rho_0/2^{\text{iter}-1} =$ 0.0078125 Hz. If the traditional ergodic method is used, the iteration is 5121, while the iteration of the bisectional method is 38.

Assuming that the Doppler is $\hat{\theta}$, then the compensated received signal can be expressed as

$$\hat{\mathbf{y}} = \hat{\boldsymbol{\Theta}}^H\boldsymbol{\Theta}\mathbf{H}\mathbf{s} + \hat{\boldsymbol{\Theta}}^H\mathbf{w} = \mathbf{H}\mathbf{s} + \hat{\mathbf{w}}. \tag{12}$$

*2) Channel Estimation:* Channel estimation plays an essential role in coherent communication, which provides priority information for the channel equalizer. After Doppler compensation, the received vectors in the frequency domain can be written as [51]

$$\hat{\mathbf{v}}_m = \mathbf{A}_m\mathbf{h} + \boldsymbol{\omega} \tag{13}$$

---

**Algorithm 1** Doppler Estimation Algorithm

**Input:** the received time domain signal $\mathbf{y}$, the zero vector selection matrix $\mathbf{P}_z$, the absolute value of the initial tentative Doppler $\epsilon_0$, the number of vector $(M)$, the size of vector $(N)$, bandwidth $B$;

**Output:** estimated Doppler estimate $\hat{\theta}$;

**Initialize** $\rho_0$, $iter$, $\theta_{\min} = -1 \times \epsilon_0$, $\theta_{\max} = 1 \times \epsilon_0$;
**for** $k$=$1{:}M$ **do**
  **perform** (9);
**end**
**for** $g = 1 : iter$ **do**
  $\rho = \rho_0/2^{g-1}$;
  $\theta = \theta_{\min}{:}\rho{:}\theta_{\max}$;
  **perform** (11);
  $\theta_{\min} = \hat{\theta} - \rho/2$;
  $\theta_{\max} = \hat{\theta} + \rho/2$;
**end**

---

where $\boldsymbol{\omega}$ is the ambient noise in the frequency domain, $\mathbf{A}_m = \mathbf{U}_m^H\mathbf{D}_m\Gamma_m$ is an $M \times L$ matrix with $\mathbf{U}_m = \mathbf{F}_M\boldsymbol{\Lambda}_M^m$, $\mathbf{D}_m = \mathrm{diag}(\mathbf{U}_m\mathbf{x}_m)$, and $\Gamma_m = (\mathbf{I}_M \odot \mathbf{i}_N^T(m))\mathbf{F}_K(:, 0 : L-1)$. The notation $\boldsymbol{\Lambda}_M^m$ is defined as $\boldsymbol{\Lambda}_M^m = \mathrm{diag}(1, e^{-j2\pi m/K}, \ldots, e^{-j2\pi m(M-1)/K})$.

In our design, the pilot vectors are utilized to perform channel estimation. By stacking all the pilot vectors together, based on (13), the channel model is written as

$$\mathbf{v}_p = \mathbf{A}_p\mathbf{h} + \boldsymbol{\omega}_p \tag{14}$$

where $\mathbf{v}_p = (\mathbf{v}_{p_0}^T, \ldots, \mathbf{v}_{p_{P-1}}^T)^T$, $\mathbf{A}_p = (\mathbf{A}_{n_0^p}^T, \ldots, \mathbf{A}_{n_{P-1}^p}^T)^T$, and $\boldsymbol{\omega}_p = (\boldsymbol{\omega}_{n_0^p}, \ldots, \boldsymbol{\omega}_{n_{P-1}^p})^T$.

The least-square method is adopted to measure the underwater acoustic channel shown in (14), it is measured as

$$\hat{\mathbf{h}} = \left(\mathbf{A}_p^H\mathbf{A}_p\right)^{-1}\mathbf{A}_p^H\mathbf{v}_p. \tag{15}$$

Equation (15) needs a matrix-inverse process, and it needs a long time to be measured, which results in a nonreal-time system. Fortunately, the pilot vectors are known and remain the same among different OSDM symbols, as a result, the matrix $(\mathbf{A}_p^H\mathbf{A}_p)^{-1}\mathbf{A}_p^H$ is constant. Inspired by this, the matrix $(\mathbf{A}_p^H\mathbf{A}_p)^{-1}\mathbf{A}_p^H$ is measured and written into a ".c" file in advance. Measuring the channel becomes a matrix multiplying a vector, and the computational complexity reduces significantly. The computational complexity of the proposed method is affordable in an embedded system.

After the channel estimate is obtained, the time-domain channel is transformed to the frequency domain via DFT

$$\boldsymbol{\eta} = (\eta_0, \ldots, \eta_{K-1}) = \mathbf{F}_K(:, 0 : L-1)\hat{\mathbf{h}}. \tag{16}$$

Since notation $\mathbf{F}_K(:, 0 : L-1)$ is constant, and it is written into a ".c" file in advance.

*3) Channel Equalization:* The frequency-domain equalizer is usually adopted since it has lower computational complexity. It should be noticed that, in a one-tap frequency-domain equalizer, the complexity is mainly the complexity of the DFTs,

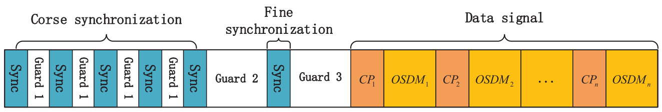


Fig. 4. Structure of one OSDM frame.

hence, a minimum mean square error (MMSE) equalizer is adopted in our OSDM MODEM without hurting the real-time implementation feasibility. The formulation of the equalized symbols in the $m$th vector is [47]

$$\hat{\mathbf{x}}_m = \mathbf{\Lambda}_M^{mH}\mathbf{F}_M^H(\hat{\mathbf{H}})_m^{-1}\mathbf{F}_M\mathbf{\Lambda}_M^m\mathbf{v}_{d_m} \tag{17}$$

where $(\hat{\mathbf{H}})_m^{-1} = \text{diag}\{1/(\eta_m + \sigma^2), 1/(\eta_{N+m} + \sigma^2), \ldots, 1/(\eta_{(M-1)N+m)} + \sigma^2)\}$. One may see that the frequency-domain equalizer avoids the matrix inverse. Since the matrix $\mathbf{F}_M$ is constant, it is written into a ".c" file in advance.

If a single-input–multiple-output (SIMO) underwater acoustic system is adopted, the multichannel combining can be expressed as

$$\hat{\mathbf{x}}_m = \sum_{i=1}^{\chi}\left(\mathbf{\Lambda}_M^{mH}\mathbf{F}_M^H(\hat{\mathbf{H}})_{m,i}^{-1}\mathbf{F}_M\mathbf{\Lambda}_M^m\mathbf{v}_{d_m,i}\right) \tag{18}$$

notation $(\hat{\mathbf{H}})_{m,i}^{-1}$ is defined as

$$(\hat{\mathbf{H}})_{m,i}^{-1} = \text{diag}\left(\frac{\eta_{m,i}^*}{\sum_{i=1}^{\chi}|\eta_{m,i}|^2 + \sigma_i^2}, \ldots, \frac{\eta_{(M-1)N+m,i}^*}{\sum_{i=1}^{\chi}|\eta_{(M-1)N+m,i}|^2 + \sigma_i^2}\right). \tag{19}$$

Notation $i$ in (18) and (19) denotes the index of the hydrophone, and $\chi$ denotes the number of total hydrophones. It should be noticed that when $\sigma^2 = 0$, the MMSE equalizer reduces to the zero-forcing (ZF) equalizer.

## C. Frame Format Design

The structure of one OSDM frame is shown in Fig. 4, including coarse synchronization, guard intervals, fine synchronization, and OSDM symbols. Usually, synchronization signals have excellent autocorrelation. The purpose of the guard interval is to prevent multipath. Specifically, the linear frequency modulation signal is used as synchronization with a duration of 53.13 ms. The durations of guard interval 1, guard interval 2, and guard interval 3 are 35.20, 176.67, and 176.67 ms, respectively. For instructions on how to synchronize one frame and capture the beginning of data, refer to our previous work in [7]. After the fine synchronization and subsequent guard interval, the OSDM symbols with CP inserted at their beginning are generated. There are 32 OSDM symbols in one frame.

In fact, in our MODEM design, the double-buffered method and enhanced direct memory access (EDMA) are utilized. In the transmitter, when one buffer is transmitting one OSDM signal, the other buffer is generating the next OSDM signal. In the receiver, when one buffer is receiving one OSDM signal, the other buffer is processing the previous OSDM signal. The length of one buffer is equal to the duration of one OSDM and its CP. The mechanism of the double-buffered method and EDMA can be found in our previous work in [7].

TABLE II
RUNTIME OF SPECIFIC PROCESSES

| Process module | Value |
|---|---|
| 45-point DFT and IDFT ($\mu$s) | 19.1 |
| Polar encoding (ms) | 16.67 |
| Polar decoding (ms) | 4.55 |
| Doppler estimation and compensation (ms) | 34.7464 |
| Channel estimation (ms) | 0.6025 |
| Channel equalization (ms) | 6.7096 |

## D. Evaluation of Runtime

In our MODEM design, the OMAPL138 processor which contains a C674x DSP and an ARM processor is adopted. The details about OMAPL138 are introduced in [7]. To improve the CPU's efficiency, the integrated digital signal processing library is used. For example, the functions *cossp()* and *sinsp()* are used to generate carrier and matrix $\mathbf{\Lambda}_M^m$. The pulse shaping and lowpass filter are performed via convolution, and the convolution is implemented by fast Fourier transform (FFT) and inverse FFT (IFFT). The FFT and IFFT processes are implemented by *DSPF_sp_fftSPxSP()* and *DSPF_sp_ifftSPxSP()*. The function *DSPF_sp_mat_mul_cplx()* is used for matrix or vector multiplication which is frequently called in channel estimation, channel equalization, DFT, and IDFT. In addition to the integrated digital signal processing library, some functions written by ANSI C are optimized by hand, for example, complex vectors multiplying functions, measuring the maximum value, and so on.

The runtime of each component is shown in Table II.

The runtime of generating one OSDM symbol shown in the top part of Fig. 1 is 35.71 ms, and the runtime of decoding one OSDM symbol using two channels shown in the bottom part of Fig. 1 is 100.00 ms. Since the duration of one OSDM and its CP is 176.67 ms, it can be seen that our OSDM MODEM is a real-time MODEM. One may notice that the runtime of demodulation for a 2 × 2 MIMO-OSDM MODEM is about 164 ms, implementing an MIMO-OSDM MODEM is possible under the SIMO-OSDM framework.

# III. HARDWARE DESIGN

The prototype of our OSDM MODEM is shown in Fig. 5. It consists of the transducers, the case, and the cable. The dry end is sealed into the case, including the DSP, analog circuit board, power amplifier, and battery. Our MODEM supports two transducers that support SIMO and MIMO systems. The information is exchanged via the cable using Ethernet. Also, the power supply or battery charging can be carried out via the cable. The detailed descriptions of the DSP, preamplifier, power amplifier, and bandpass filter are introduced in Sections III-A–III-C. In our OSDM MODEM, the SIMO communication system is adopted, where two transducers receive signals and only one transducer transmits signals.

Fig. 5. Prototype of our OSDM MODEM.

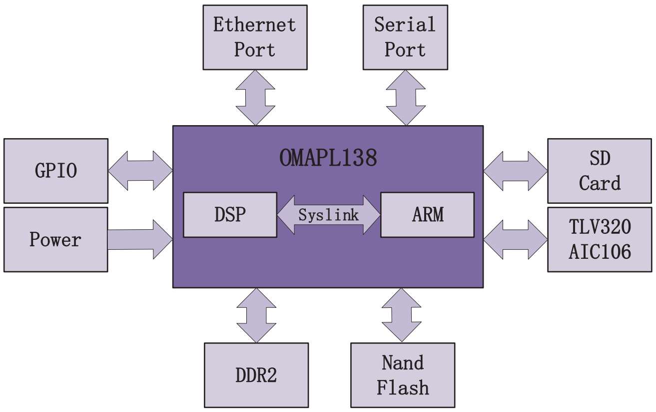


Fig. 6. Main structure we used for the OMAPL138.

## A. Digital Signal Processor and Peripheral

Our OSDM MODEM chooses an OMAPL138 processor which has the balance between computation and power consumption. The OMAPL138 contains one TMS320C6748 and one ARM dual core, as shown in Fig. 6. The TMS320C6748 core is mainly used for modulation and demodulation, while the ARM core which runs in a Linux operating system is used to exchange messages via Ethernet, and record received signals into an SD card. The information exchange between the two cores is called syslink. The general purpose input/output (GPIO) is used to adjust the gain of the preamplifier, to control the relay that determines if the MODEM works in transmitting mode or receiving mode. The capacity of external DDR2 is 128 MB which can be accessed by both TMS320C6748 and ARM. Since the communication bandwidth of our MODEM works in audio frequency, the TLV320AIC3106 audio chip that integrated ADCs and DACs is adopted directly. The TLV320AIC3106 supports sampling rates from 8 to 96 kHz, and it supports two ADCs and two DACs, which are conveniently designed for SIMO or MIMO systems. The syslink is used for sharing data between DSP and ARM. In our OSDM MODEM, when the acoustic data is achieved via the TLV320AIC3106, it will pass through the shared memory; when the DSP core is demodulating, the ARM core is recording the raw acoustic data into an SD card simultaneously. As a result, the MODEM also acts as a self-contained hydrophone. By using the function of a self-contained hydrophone, we can analyze the signal offline.

## B. Power Amplifiers

Considering the working bandwidth of our MODEM is less than 20 kHz, an efficient class-D power amplifier named TPA3251 is used. Fig. 7 is the schematic circuit of the TPA3251 in our MODEM. Since our MODEM needs only

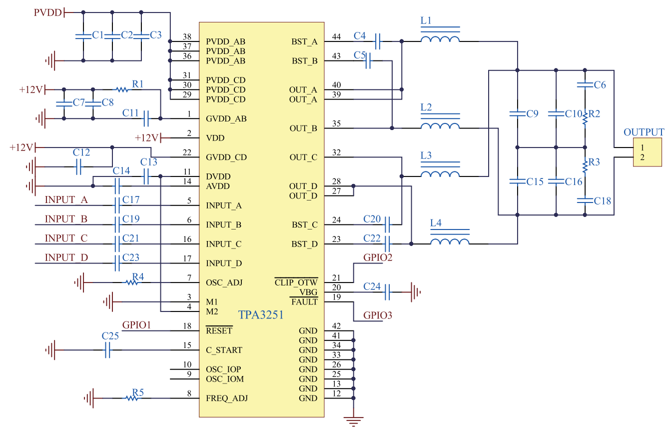


Fig. 7. Schematic circuit of the TPA3251.

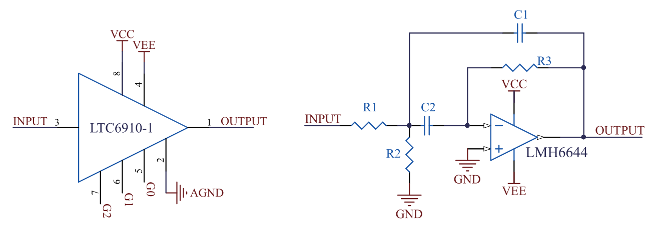


(a) (b)

Fig. 8. Schematic circuit. (a) Schematic circuit of the LTC6910-1. (b) Schematic circuit of a second-order bandpass filter.

one transmitter, the power amplifier is configured in the PBTL mode, in which the maximum power can reach 350 W at 10% total harmonic distortion (THD) + $N$ or 285 W at 1% THD + $N$, while the maximum power of the TDA7498E can only reach 220 W [7]. The power amplifier integrates components that prevent over-temperature and over-current. Pin 21, Pin 19, and Pin 18 are connected to the TMS320C6748 to monitor the power amplifier. In fact, the power amplifier also can be configured in a stereo mode that supports an MIMO system. In a word, the merit of the TPA3251 power amplifier is threefold, first, the high power can be used to reach a long communication range; second, the over-temperature and over-current components can protect the OSDM MODEM; third, the size of the power amplifier is small which enables to design smart MODEMs.

## C. Preamplifiers and Bandpass Filters

Due to the severe propagation loss and absorption and ambient noise with a large bandwidth in the underwater acoustic channels, the received signal is quite weak. To improve the received SNR, a bandpass filter and a preamplifier are adopted in our OSDM MODEN. The LTC6910-1 is adopted to amplify the received signal, and an eight-order bandpass filter based on Chebyshev [7] is adopted to cancel noise whose bandwidth is located outside our MODEM's bandwidth. The gain of the LTC6910-1 is adjustable using a 3-bit digital input to select gains of 0, 1, 2, 5, 10, 20, 50, and 100 V/V. The bandwidth of the LTC6910-1 is up to 11 MHz. By using digital control, automatic gain control (AGC) is easily implemented. Fig. 8(a) is the schematic circuit of the LTC6910-1, and one second-order bandpass filter is shown in Fig. 8(b).

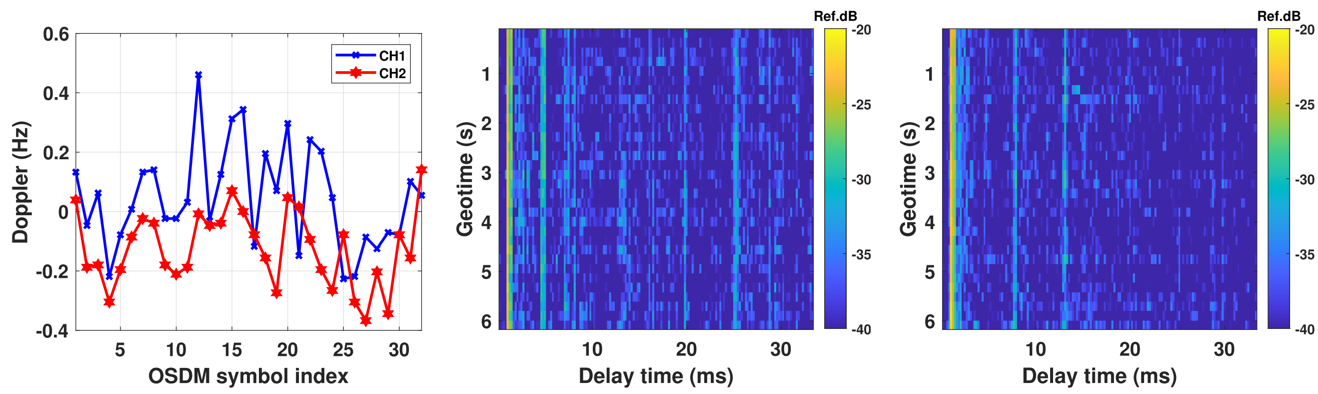


Fig. 9. Doppler estimation and CIRs in case15. (a) Doppler estimation from the first frame. (b) CIR of CH1. (c) CIR of CH2.

TABLE III
PARAMETERS OF OUR OSDM MODEM

| Parameter | Notation | Value |
|---|---|---|
| Number of receivers | $\chi$ | 2 |
| Sample frequency (kHz) | $f_s$ | 48 |
| Carrier frequency (kHz) | $f_c$ | 11 |
| Bandwidth (kHz) | $B$ | 4.8 |
| Mapping constellation | $Q$ | QPSK |

TABLE IV
DIFFERENT SCENARIOS AND CORRESPONDING DATA RATES

| Parameters | Zero vector #2 | Zero vector #3 | Zero vector #5 |
|---|---|---|---|
| Pilot vector #4 | case1 (7.64/5.73 kbps) | case6 (7.44/5.58 kbps) | case11 (7.05/5.29 kbps) |
| Pilot vector #6 | case2 (6.96/5.22 kbps) | case7 (6.77/5.08 kbps) | case12 (6.40/4.80 kbps) |
| Pilot vector #8 | case3 (6.33/4.75 kbps) | case8 (6.16/4.62 kbps) | case13 (5.80/4.35 kbps) |
| Pilot vector #10 | case4 (5.76/4.32 kbps) | case9 (5.59/4.19 kbps) | case14 (5.24/3.93 kbps) |
| Pilot vector #12 | case5 (5.27/3.92 kbps) | case10 (5.05/3.79 kbps) | case15 (4.72/3.54 kbps) |

Compared with our previous work in [7], our preamplifier does not need a DAC to control the gain, instead, three digital pins can control the gain. Since the OMAPL138 contains rich digital pins, avoiding the DAC results in a lower cost. Moreover, the structure of the bandpass filter makes it easy to adjust the center frequency and bandwidth. The size and power consumption of the bandpass filter in the design are smaller than those in [7].

## IV. EXPERIMENTAL RESULTS AND ANALYSIS

To accommodate different underwater environments, the performance of our proposed OSDM MODEM under different pilot vectors, data vectors, and zero vectors is investigated. An offshore sea trial experiment was conducted in Wuyuan Bay, Xiamen, China, to verify the performance of different settings. In addition, to verify the effectiveness and reliability of our OSDM MODEM under slow time-varying channels, two other sea trials were conducted in Xiamen Harbor and the Taiwan Strait, respectively. The three sea trials are introduced and analyzed in Sections IV-A–IV-C.

The parameters of our proposed OSDM MODEM are shown in Table III. The sampling frequency is 48 000 Hz, the carrier frequency is 11 000 Hz, the bandwidth is 4800 Hz, and the QPSK mapping method is used. To reduce the error further, polar encoding and decoding methods [52] are used with the length of 768/1024, and the coding rate is 3/4. The CIRs from the transmitter to the lower receiver and the upper receiver are denoted as CH1 and CH2, respectively.

### *A. First Sea Trial in Wuyuan Bay*

To compare the performance of our OSDM MODEM with the 15 different configurations, the first sea trial was conducted in Wuyuan Bay, Xiamen, China. The average SNR was 21.63 dB. The 15 configurations of the different parameters are shown in Table IV, and the different data rates before channel decoding and after channel decoding are also shown in Table IV. To better describe, the scenarios of different parameters are denoted as case1 to case15 shown in Table IV.

The transducers were set at the depths of 2 and 6 m for both OSDM MODEMs, and the horizontal distance between the two MODEMs was about 1 km. Signals from case1 to case15 are modulated by our OSDM MODEM and transmitted ten times for each case.

Fig. 9(a) shows the Doppler estimation of 32 symbols from the first frame in case15. One may see that the range of Doppler is from −0.4 to 0.5 Hz, and the reason is that the receiver and the transmitter are stationary and the Doppler shift is caused by the heavy current. In addition, it can be seen that the tendency of Doppler from different channels shows similar.

Fig. 9(b) and (c) shows the CIRs after Doppler compensation from the first frame in case15. The least-square method is adopted for channel estimation shown in (15), and the channel length is 33.3 ms. One may see that from Fig. 9 that the complex multipath is obvious with the maximum delay of 30 ms, and the structures of the two channels are quite different. Such channel diversity can be used to improve communication performance. It can also be seen that the channels show slow time-varying. The long time-delay channel may be caused by the closed experimental area.

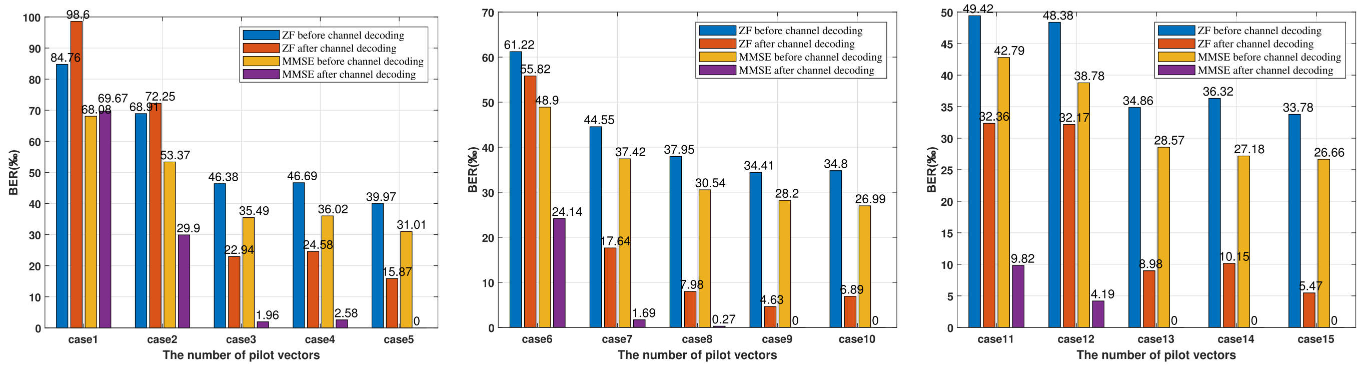


(a) (b) (c)

Fig. 10. Results of different parameters. (a) Results obtained from case1 to case5. (b) Results obtained from case6 to case10. (c) Results obtained from case11 to case15.

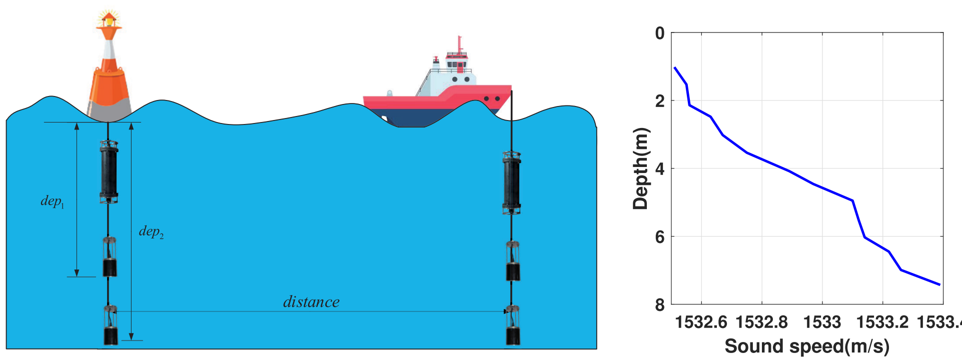


(a) (b)

Fig. 11. Diagram of deployment and the SSP from Xiamen Harbor. (a) Diagram of deployment. (b) SSP.

Finally, the results of all kinds of configurations are shown in Fig. 10. The channel length is set to 33.33 ms, and the parameter $\sigma^2$ in (19) is set to 0.01. Focusing on the same number of zero vectors and the different number of pilot vectors, the larger number of pilot vectors leads to lower BER, the reason is that more pilot vectors lead to accurate channel estimation when the least-square method is used. For example, when the number of zero vectors is 3, the average BER before polar decoding obtained by MMSE from case6 and case10 is 48.90‰ and 26.99‰, respectively. From the point of view of the same number of pilot vectors and the different number of zero vectors, the higher number of zero vectors leads to lower BER. The reason is that the more zero vectors result in better Doppler estimation shown in (11). For example, when the number of pilot vectors is 12, the average BER before polar decoding obtained by MMSE from case5 and case15 is 42.97‰ and 26.66 ‰, respectively.

From Fig. 10, it can be concluded that, first of all, our proposed OSDM MODEM can handle the relative long-time and slow time-varying channel. The more zero vectors and pilot vectors achieve lower BER, unfortunately, the data rate is decreased. In our OSDM MODEM, the parameters can be adjusted to get the balance between BER and data rate. Moreover, the MMSE equalizer achieves lower BER than that obtained by the ZF equalizer. In addition, the polar decoding method can correct the error furthermore, especially when the BER before polar decoding is less than about $3e-3$, the polar decoding strategy will correct all the error bits, which leads to free-error communication. Finally, although the Doppler shift is insignificant, the number of zero vectors should be greater than 5 to guarantee considerable communication performance.

## B. Second Trial in Xiamen Harbor

The second experiment was conducted in Xiamen Harbor, Xiamen, China. The configuration of our OSDM MODEM used case13 where the number of zero vectors was 5, and the number of pilot vectors was 8, thus the maximum channel length can be reached at 26.67 ms. The average depth was 12 m, the average air temperature was 32.7 °C, and the average wind velocity was 4.14 m/s. One MODEM was suspended to a ship, and the other was suspended to a buoy. The transducers were set at the depths of 4 and 8 m for both OSDM MODEMs shown in Fig. 11(a). The horizontal distance between the two MODEMs was 1.5 km. The sound speed profile (SSP) is shown in Fig. 11(b), and the gradient of sound velocity shows a slight positive. The average SNR was 18.70 dB. In this experiment, 12 frames were transmitted, and the total binary data was 294 912.

Fig. 12(a) shows the Doppler estimation of 32 symbols from the first frame, and the range of Doppler is from $-2$ to 3 Hz. Fig. 12(b) and (c) shows the CIRs from two channels after Doppler compensation, respectively. The channel length is 10.5 ms, and the delay of multipath is less than 5 ms.

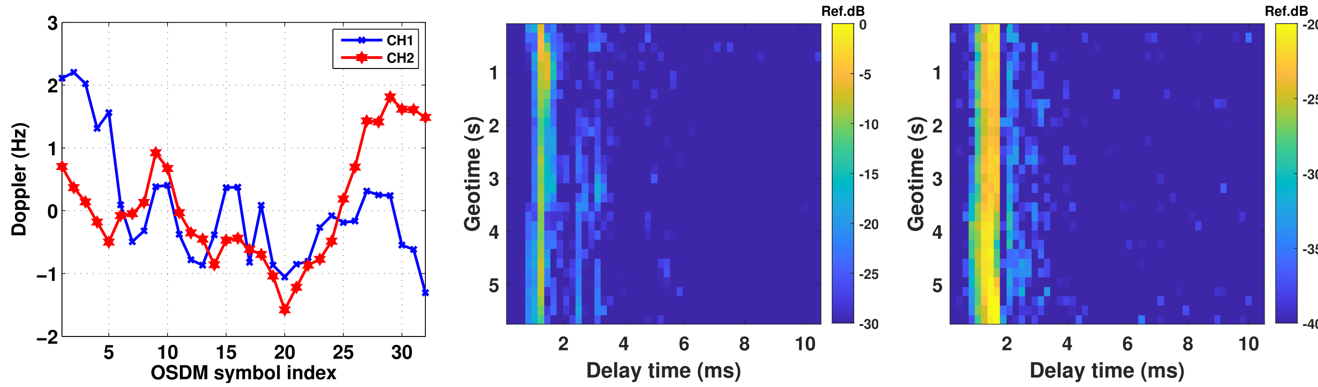


(a) (b) (c)

Fig. 12. Doppler estimation and CIRs from the first data frame. (a) Doppler estimation. (b) CIR of CH1. (c) CIR of CH2.

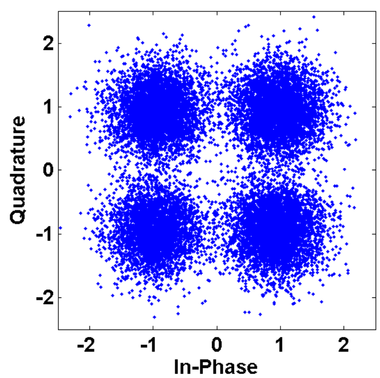


Fig. 13. Equalizer output scatterplot of OSDM MODEM in Xiamen Harbor from the first data frame.

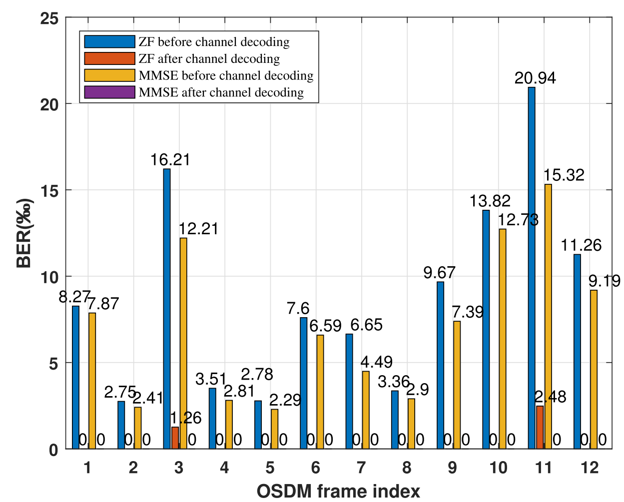


Fig. 14. BER of OSDM frames before and after polar decoding.

The channels show the time-varying characteristic which may be caused by heavy currents and heavy wind.

The equalizer output scatterplot in Fig. 13 is obtained by MRC from the equalizer in (19). It can be seen that the equalizer output scatterplot is clearly separated, which implies low BER.

Finally, all 12 frames are analyzed in terms of BER before and after polar decoding. The result is shown in Fig. 14. The maximum BER using the ZF equalizer before and after channel decoding is 20.94‰ and 2.75‰, respectively. The maximum BER using the MMSE equalizer before and after channel decoding is 12.73‰ and 0‰, respectively. The MMSE equalizer outperforms the ZF equalizer. Since the experimental field was in the main lane, there were different kinds of noise, such as impulsive noise, ship noise, and so on, and the noisy underwater environment caused a nonnegligible error bit. Fortunately, the final BER using the MMSE equalizer after polar decoding achieves free error.

### *C. Third Trial in the Taiwan Strait*

To further verify the validity of our OSDM MODEM in different marine environments, one data frame containing the 32 OSDM symbols was transmitted in the Taiwan Strait. The average depth of the field was 49.9 m, the average air temperature was 32.5 °C, and the average wind velocity was 1.86 m/s. The two MODEMs were suspended at two boats, and the depths of the two transducers were 7 and 12 m, respectively. The horizontal distance between the two MODEMs was 5 km. The average SNR was 12.86 dB. The SSP is shown in Fig. 15(a), and the sound speed varied within 5 m/s. It should be noticed that the sound channel axis [53] appears at 25 m.

Fig. 15(b) shows the BER among all the OSDM symbols. The average BER using the ZF equalizer before and after channel decoding is $2.20 \times 10^{-3}$ and $9.35 \times 10^{-4}$, respectively. The average BER using the MMSE equalizer before and after channel decoding is $1.56 \times 10^{-3}$ and 0, respectively. Fig. 15(c) shows the equalizer output scatterplot which also shows certain separations. Our OSDM MODEM achieved error-free transmission with a data rate of 4.35 kb/s over 5 km.

According to the three experiments, our OSDM MODEM achieved satisfactory performance under slow time-varying channels. Compared to our previous OFDM MODEM work [7], our OSDM MODEM has lower PAPR, higher data rate, lower bit error rate, and achieves error-free transmission over longer distances.

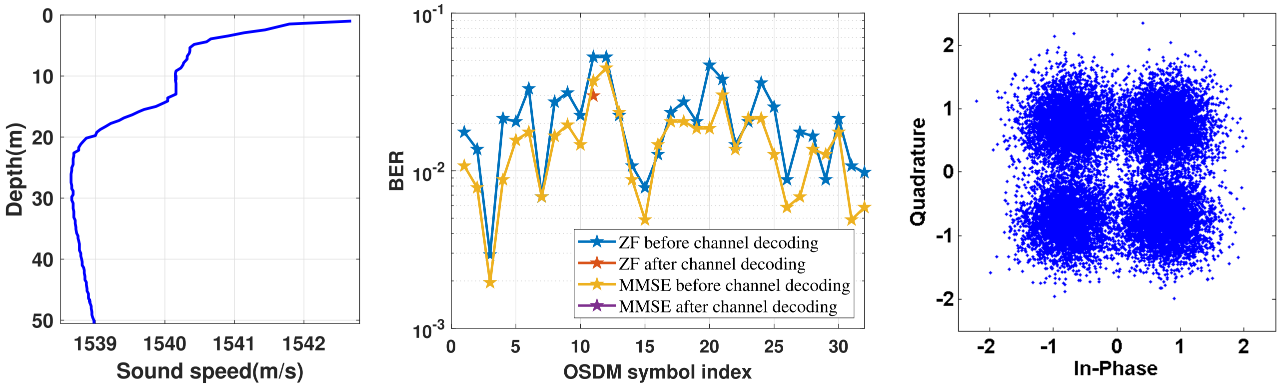


(a) (b) (c)

Fig. 15. SSP, BER, and equalizer output scatterplot of the experiment in the Taiwan Strait. (a) SSP from the Taiwan Strait. (b) BER of OSDM symbols before and after channel decoding. (c) Equalizer output scatterplot of the experiment in the Taiwan Strait.

## V. Conclusion

The OSDM is a compromise between single-carrier communication and multicarrier communication. In this article, an OSDM underwater acoustic MODEM was researched and designed, as far as we know, it was the first trial to design a real-time underwater acoustic OSDM MODEM. The software and hardware design for our OSDM MODEM were introduced in detail. In the software design, OSDM modulation, OSDM demodulation, Doppler estimation and compensation, channel estimation, and channel equalization were carefully researched and implemented; in the hardware design, the preamplifier, the bandpass filter, and the power amplifier were introduced. Different from the theoretical analysis, the modulation and demodulation were performed vector by vector to avoid large matrix multiplications. Some constant matrices were generated and saved to RAM in advance, so the runtime of the embedded systems was reduced. Moreover, some functions from the digital signal processing library were introduced to reduce runtime further. To accommodate different underwater acoustic channels and get the balance between BER and data rate, our proposed OSDM MODEM was able to set different numbers of pilot vectors and zero vectors. Three sea trials demonstrated the effectiveness of the proposed OSDM MODEM. Especially, our OSDM MODEM achieved free error after channel decoding when the number of zero vectors was 5, and the number of pilot vectors was no less than 8, the corresponding data rate was more than 4.35 kb/s after channel decoding. Satisfactory performance was achieved under slow time-varying acoustic channels.

## VI. Future Work

In order to enrich some functionality of our proposed MODEM, we will consider the following future work:

1) Based on the structure, a soft-defined MODEM will be considered in the future.
2) The impulsive noise usually appears in shallow water near shore, which would degrade the communication performance. In the future, impulsive noise cancellation will be implemented.
3) Our OSDM MODEM was successfully applied on the underwater static scenes with a small Doppler effect, in the future, the underwater mobile scenes with a large Doppler effect will be considered, for example, a FARROW filter can be used to compensate for the large Doppler with low computational complexity.
4) The strategy that automatically changes the number of pilot vectors, and the number of zero vectors based on the underwater acoustic channel will be considered and researched.
5) Network protocols will be implemented in the ARM core to support underwater network technology for UWSNs.

## References


[1] M. Ahmed, M. Salleh, and M. I. Channa, "Routing protocols based on protocol operations for underwater wireless sensor network: A survey," *Egyptian Informat. J.*, vol. 19, no. 1, pp. 57–62, Mar. 2018.
[2] M. Khalid et al., "A survey of routing issues and associated protocols in underwater wireless sensor networks," *J. Sensors*, vol. 2017, pp. 1–17, May 2017.
[3] G. Han, X. Long, C. Zhu, M. Guizani, and W. Zhang, "A high-availability data collection scheme based on multi-AUVs for underwater sensor networks," *IEEE Trans. Mobile Comput.*, vol. 19, no. 5, pp. 1010–1022, May 2020.
[4] G. Qiao, Q. Liu, S. Liu, B. Muhammad, and M. Wen, "Symmetric connectivity of underwater acoustic sensor networks based on multi-modal directional transducer," *Sensors*, vol. 21, no. 19, pp. 6548–6571, 2021.
[5] X. Su, I. Ullah, X. Liu, and D. Choi, "A review of underwater localization techniques, algorithms, and challenges," *J. Sensors*, vol. 2020, pp. 1–24, Jan. 2020.
[6] I. Kulkarni and D. Pompili, "Task allocation for networked autonomous underwater vehicles in critical missions," *IEEE J. Sel. Areas Commun.*, vol. 28, no. 5, pp. 716–727, Jun. 2010.
[7] Y. Zhou and F. Tong, "Research and development of a highly reconfigurable OFDM MODEM for shallow water acoustic communication," *IEEE Access*, vol. 7, pp. 123569–123582, 2019.
[8] T.-H. Won and S.-J. Park, "Design and implementation of an omni-directional underwater acoustic micro-modem based on a low-power micro-controller unit," *Sensors*, vol. 12, no. 2, pp. 2309–2323, Feb. 2012.
[9] J. Jeon, S. Hwangbo, H. Peyvandi, and S. Park, "Design and implementation of a bidirectional acoustic micro-modem for underwater communication systems," in *Proc. Oceans*, Oct. 2012, pp. 1–4.
[10] W. Lee, J. Jeon, and S. Park, "Micro-modem for short-range underwater communication systems," in *Proc. Oceans St. John's*, Sep. 2014, pp. 1–4.
[11] J. Younce, A. Singer, T. Riedl, B. Landry, A. Bean, and T. Arikan, "Experimental results with HF underwater acoustic modem for high bandwidth applications," in *Proc. 49th Asilomar Conf. Signals, Syst. Comput.*, Nov. 2015, pp. 248–252.
[12] M. S. Martins, J. Cabral, G. Lopes, and F. Ribeiro, "Underwater acoustic modem with streaming video capabilities," in *Proc. OCEANS Genova*, May 2015, pp. 1–7.

[13] R. Zhao, H. Mei, X. Shen, W. Fang, and H. Wang, "Underwater acoustic network node design and anechoic pool network experimentation with five nodes," in *Proc. IEEE/OES China Ocean Acoust. (COA)*, Jan. 2016, pp. 1–5.

[14] W. Lei, D. Wang, Y. Xie, B. Chen, X. Hu, and H. Chen, "Implementation of a high reliable chirp underwater acoustic modem," in *Proc. Oceans Yeosu*, May 2012, pp. 1–5.

[15] H. Zhang, S. Xiong, Z. Yue, and Z. Wang, "Sea trials of an underwater acoustic network in the East China Sea 2015," in *Proc. IEEE/OES China Ocean Acoust. (COA)*, Jan. 2016, pp. 1–5.

[16] S. Zheng, F. Tong, B. Li, Q. Tao, A. Song, and F. Zhang, "Design and evaluation of an acoustic modem for a small autonomous unmanned vehicle," *Sensors*, vol. 19, no. 13, pp. 2923–2934, 2019.

[17] I. Kochanska, R. Salamon, J. H. Schmidt, and A. M. Schmidt, "Study of the performance of DSSS UAC system depending on the system bandwidth and the spreading sequence," *Sensors*, vol. 21, no. 7, pp. 2484–2504, 2021.

[18] S. Indriyanto and I. Y. M. Edward, "Ultrasonic underwater acoustic modem using frequency shift keying (FSK) modulation," in *Proc. 4th Int. Conf. Wireless Telematics (ICWT)*, Jul. 2018, pp. 1–4.

[19] Y. Su, L. Dong, Z. Zhou, X. Liu, and X. Wei, "A general embedded underwater acoustic communication system based on advance STM32," *IEEE Embedded Syst. Lett.*, vol. 13, no. 3, pp. 90–93, Sep. 2021.

[20] T. Husøy, M. Pettersen, B. Nilsson, T. Öberg, N. Warakagoda, and A. Lie, "Implementation of an underwater acoustic modem with network capability," in *Proc. OCEANS IEEE Spain*, Jun. 2011, pp. 1–10.

[21] L. Xu and S. Yan, "Design of underwater acoustic modems through high performance DSPs," in *Proc. Int. Conf. Underwater Netw. Syst.*, 2014, pp. 1–2.

[22] J. A. Neasham, G. Goodfellow, and R. Sharphouse, "Development of the 'Seatrac' miniature acoustic modem and USBL positioning units for subsea robotics and diver applications," in *Proc. OCEANS Genova*, 2015, pp. 1–8.

[23] B. Peng and H. Dong, "DSP based real-time single carrier underwater acoustic communications using frequency domain turbo equalization," *Phys. Commun.*, vol. 18, pp. 40–48, Mar. 2016.

[24] L. Shen, B. Henson, Y. Zakharov, and P. Mitchell, "Digital self-interference cancellation for full-duplex underwater acoustic systems," *IEEE Trans. Circuits Syst. II, Exp. Briefs*, vol. 67, no. 1, pp. 192–196, Jan. 2020.

[25] T. Shimura, Y. Kida, and M. Deguchi, "High-rate underwater acoustic communication system for SHINKAI6500," in *Proc. IEEE/OES Auto. Underwater Vehicle Workshop (AUV)*, Nov. 2018, pp. 1–5.

[26] J. Xi, S. Yan, L. Xu, and C. Hou, "Sparsity-aware adaptive turbo equalization for underwater acoustic communications in the Mariana trench," *IEEE J. Ocean. Eng.*, vol. 46, no. 1, pp. 338–351, Jan. 2021.

[27] J. Li, J. Halt, and Y. R. Zheng, "Utilizing Janus for very high frequency underwater acoustic modem," in *Proc. Global Oceans, Singap. U.S. Gulf Coast*, Oct. 2020, pp. 1–6.

[28] H. Nam and S. An, "Low-power based coherent acoustic modem for emerging underwater acoustic sensor networks," *Wireless Pers. Commun.*, vol. 57, no. 2, pp. 291–309, Mar. 2011.

[29] A. Sánchez, S. Blanc, P. Yuste, A. Perles, and J. J. Serrano, "An ultra-low power and flexible acoustic modem design to develop energy-efficient underwater sensor networks," *Sensors*, vol. 12, no. 6, pp. 6837–6856, May 2012.

[30] H. Yan et al., "DSP implementation of SISO and MIMO OFDM acoustic modems," in *Proc. OCEANS IEEE SYDNEY*, May 2010, pp. 1–6.

[31] H. Yan et al., "DSP based receiver implementation for OFDM acoustic modems," *Phys. Commun.*, vol. 5, no. 1, pp. 22–32, Mar. 2012.

[32] G. Qiao, S. Z. Liu, F. Zhou, and Z. X. Sun, "Experimental study of long-range shallow water acoustic communication based on OFDM-modem," in *Advanced Materials Research*, vol. 546. Zurich, Switzerland: Trans Tech Publications, 2012, pp. 1308–1313.

[33] G. Qiao, S. Liu, Z. Sun, and F. Zhou, "Full-duplex, multi-user and parameter reconfigurable underwater acoustic communication modem," in *Proc. OCEANS San Diego*, Sep. 2013, pp. 1–8.

[34] L. Ma, G. Qiao, and S. Liu, "HEU OFDM-modem for underwater acoustic communication and networking," in *Proc. Int. Conf. Underwater Netw. Syst.*, 2014, pp. 1–5.

[35] Z. Peng et al., "NAMS: A networked acoustic modem system for underwater applications," in *Proc. OCEANS MTS/IEEE KONA*, Sep. 2011, pp. 1–5.

[36] L. Wang, P. Qiao, J. Liang, T. Chen, X. Wang, and G. Yang, "Accurate channel estimation and adaptive underwater acoustic communications based on Gaussian likelihood and constellation aggregation," *Sensors*, vol. 22, no. 6, pp. 2142–2166, 2022.

[37] L. Wu et al., "Designing an adaptive acoustic modem for underwater sensor networks," *IEEE Embedded Syst. Lett.*, vol. 4, no. 1, pp. 1–4, Mar. 2012.

[38] W. A. van Kleunen, N. A. Moseley, P. J. Havinga, and N. Meratnia, "Proteus II: Design and evaluation of an integrated power-efficient underwater sensor node," *Int. J. Distrib. Sensor Netw.*, vol. 11, no. 10, 2015, Art. no. 791046.

[39] Q. Dong, Y. Wang, and X. Guan, "The design and implementation of an underwater multimode acoustic modem for autonomous underwater vehicles," in *Proc. 37th Chin. Control Conf. (CCC)*, Jul. 2018, pp. 4201–4205.

[40] M. Chitre, I. Topor, and T. Koay, "The UNET-2 modem—An extensible tool for underwater networking research," in *Proc. Oceans Yeosu*, May 2012, pp. 1–7.

[41] E. Demirors, B. G. Shankar, G. E. Santagati, and T. Melodia, "SEANet: A software-defined acoustic networking framework for reconfigurable underwater networking," in *Proc. 10th Int. Conf. Underwater Netw. Syst.*, 2015, pp. 1–8.

[42] E. Demirors, J. Shi, R. Guida, and T. Melodia, "SEANet G2: Toward a high-data-rate software-defined underwater acoustic networking platform," in *Proc. 11th ACM Int. Conf. Underwater Netw. Syst.*, 2016, pp. 1–8.

[43] N. Suehiro, "An information transmission method using Kronecker product," in *Proc. IASTED Int. Conf. Commun. Syst. Netw.*, Sep. 2002, pp. 206–209.

[44] N. Suehiro, C. Han, and T. Imoto, "Very efficient wireless fyequency usage based on pseudo-coherent addition of multipath signals using Kronecker product with rows of DFT matrix," in *Proc. IEEE Int. Symp. Inf. Theory*, Jun./Jul. 2003, p. 385.

[45] T. Ebihara and K. Mizutani, "Underwater acoustic communication with an orthogonal signal division multiplexing scheme in doubly spread channels," *IEEE J. Ocean. Eng.*, vol. 39, no. 1, pp. 47–58, Jan. 2014.

[46] T. Ebihara and G. Leus, "Doppler-resilient orthogonal signal-division multiplexing for underwater acoustic communication," *IEEE J. Ocean. Eng.*, vol. 41, no. 2, pp. 408–427, Apr. 2016.

[47] J. Han, S. P. Chepuri, Q. Zhang, and G. Leus, "Iterative per-vector equalization for orthogonal signal-division multiplexing over time-varying underwater acoustic channels," *IEEE J. Ocean. Eng.*, vol. 44, no. 1, pp. 240–255, Jan. 2019.

[48] J. Han, L. Zhang, Q. Zhang, and G. Leus, "Low-complexity equalization of orthogonal signal-division multiplexing in doubly-selective channels," *IEEE Trans. Signal Process.*, vol. 67, no. 4, pp. 915–929, Feb. 2019.

[49] J. Han, Y. Wang, L. Zhang, and G. Leus, "Time-domain oversampled orthogonal signal-division multiplexing underwater acoustic communications," *J. Acoust. Soc. Amer.*, vol. 145, no. 1, pp. 292–300, Jan. 2019.

[50] J. Han, S. Ma, Y. Wang, and G. Leus, "Low-complexity equalization of MIMO-OSDM," *IEEE Trans. Veh. Technol.*, vol. 69, no. 2, pp. 2301–2305, Feb. 2020.

[51] J. Han, S. P. Chepuri, and G. Leus, "Joint channel and Doppler estimation for OSDM underwater acoustic communications," *Signal Process.*, vol. 170, pp. 107446–107450, May 2020.

[52] P. Trifonov, "Efficient design and decoding of polar codes," *IEEE Trans. Commun.*, vol. 60, no. 11, pp. 3221–3227, Nov. 2012.

[53] W. H. Munk, "Sound channel in an exponentially stratified ocean, with application to SOFAR," *J. Acoust. Soc. Amer.*, vol. 55, no. 2, pp. 220–226, Feb. 1974.


**Xiaoyu Yang** (Graduate Student Member, IEEE) received the bachelor's degree in marine sciences from the College of Ocean and Earth Sciences, Xiamen University, Xiamen, China, in 2021, where he is currently pursuing the Ph.D. degree in marine sciences.

His current research interests include underwater acoustic communication, underwater acoustic signal processing, and underwater acoustic network.

**Yuehai Zhou** (Member, IEEE) received the bachelor's, master's, and Ph.D. degrees in marine sciences from the College of Ocean and Earth Sciences, Xiamen University, Xiamen, China, in 2010, 2013, and 2018, respectively.

From February 2016 to January 2018, he was a Visiting Student with the Department of Electrical and Computer Engineering, The University of Alabama, Tuscaloosa, AL, USA. From 2018 to 2020, he was a Postdoctoral Researcher with the Acoustic and Navigation Laboratory, University of Haifa, Haifa, Israel. He is currently an Associate Professor with the College of Ocean and Earth Sciences, Xiamen University. His research interests include underwater acoustic signal processing, underwater acoustic network, and underwater acoustic modem design.

**Rong Wang** received the bachelor's degree in marine sciences from the College of Ocean and Earth Sciences, Xiamen University, Xiamen, China, in 2022, where she is currently pursuing the master's degree in marine sciences.

Her research interests include underwater acoustic signal processing and underwater acoustic network.

**Feng Tong** (Member, IEEE) received the Ph.D. degree in underwater acoustics from Xiamen University, Xiamen, China, in 2000.

From 2000 to 2002, he was a Postdoctoral Fellow with the Department of Radio Engineering, Southeast University, Nanjing, China. From 2003 to 2004, he was a Research Associate with the Department of Manufacturing Engineering and Engineering Management, City University of Hong Kong, Hong Kong. From 2009 to 2010, he was a Visiting Scholar with the Department of Computer Science and Engineering, University of California at San Diego, La Jolla, CA, USA. He is currently a Professor with the Department of Applied Marine Physics and Engineering, Xiamen University. His research interests include underwater acoustic communication and acoustic signal processing.

Dr. Tong is a Council Member of the Acoustical Society of China and serves on the Editorial Board for the *Journal of Marine Science and Application*.